

Unconventional higher-order topology in quasicrystals

Aoqian Shi^{1,†}, Yiwei Peng^{2,3,†}, Jiapei Jiang¹, Yuchen Peng¹, Peng Peng¹, Jianzhi Chen¹, Hongsheng Chen^{2,3}, Shuangchun Wen¹, Xiao Lin^{2,3}, Fei Gao^{2,3,*}, and Jianjun Liu^{1,*}

¹ *Key Laboratory for Micro/Nano Optoelectronic Devices of Ministry of Education & Hunan Provincial Key Laboratory of Low-Dimensional Structural Physics and Devices, School of Physics and Electronics, Hunan University, Changsha 410082, China*

² *Interdisciplinary Center for Quantum Information, State Key Laboratory of Extreme Photonics and Instrumentation, ZJU-Hangzhou Global Scientific and Technological Innovation Center, Zhejiang University, Hangzhou 310027, China*

³ *International Joint Innovation Center, The Electromagnetics Academy at Zhejiang University, Zhejiang University, Haining 314400, China*

†These authors contributed equally to this work.

*Corresponding authors: jianjun.liu@hnu.edu.cn (Jianjun Liu), gaofeizju@zju.edu.cn (Fei Gao)

ABSTRACT: Conventional two-dimensional (2D) higher-order topological insulators are characterized by higher-order topological states at the outer boundary of non-trivial regions, that is, 0D topological corner states (TCSs). In this Letter, it is found that the higher-order topological quasicrystalline insulators (HOTQIs) have non-0D TCSs arrays at the outer and inner boundaries, which breaks through the limitation of bulk-edge-corner correspondence (corresponding dimension is 2D-1D-0D). The universal theoretical framework of the multimer analysis method is improved and the difference in the average charge density is proposed as the real-space topological index, which effectively characterizes the unconventional higher-order topology in HOTQIs. Furthermore, HOTQIs and their non-0D TCSs arrays in photonic system are experimentally observed for the first time. These results offer a promising avenue for investigating TCSs with high integration and multi-region distribution and pave the way for exploring the topological phenomena and applications of photonic and phononic quasicrystals.

Keywords: higher-order topological insulator; higher-order topological quasicrystalline insulator; photonic quasicrystals

1. Introduction

Higher-order topological insulator (HOTI) based on the spatial symmetries (such as rotation symmetry and mirror symmetry) plays a unique role in fundamental and applied physics [1–21]. HOTI has been theoretically and experimentally demonstrated in electronics [1–9], photonics [10–16] and phononics [17–21]. Furthermore, HOTI provides an excellent platform for studying novel physical phenomena such as bound states in the continuum [22,23] and topological defects (such as dislocation states and disclination states) [24–28]. In previous studies of two-dimensional (2D) HOTI, according to bulk-edge-corner correspondence (corresponding dimension is 2D-1D-0D), 0D topological corner states (TCSs) exist in the corner regions of the outer boundary of the non-trivial region. It is noteworthy that, only one 0D TCS exists in each corner region. Therefore, the distribution region and integration of TCSs are limited by the periodic system. The fractal lattice has been shown to have the non-0D TCSs at the inner boundary of the fractal structure [19,20], but the TCS at its outer boundary is still consistent with that of the conventional square lattice [10–12]. This raises an interesting question: can the limitation of the bulk-edge-corner correspondence (corresponding dimension is 2D-1D-0D) at the outer boundary of the structure be broken and realize non-0D TCSs? Recently, a study theoretically found that considering the special case where long-range couplings (LRCs) stronger than nearest-neighbor couplings (NNCs) can extend the HOTI of \mathbb{Z}_2 class to \mathbb{Z} class, thus increasing the number of TCS in each corner region [29]. However, since the outer boundaries of the crystals and fractal lattices naturally only have 0D corner regions, achieving non-0D TCS at the outer boundary remains a challenging task in the general case where the NNCs are stronger than the LRCs.

Different from crystals and fractal lattices, 2D quasicrystals (quasi-periodic systems) have rotation symmetry, self-similarity, and long-range order [30–34]. Higher-order topological quasicrystalline insulator (HOTQI) based on quasicrystals exhibits unique charms that are absent in crystals and fractal lattices (such as TCSs protected by C_5 , C_8 ,

and C_{12} symmetry) [35–42], and HOTQI is expected to realize more novel topological phenomena. However, the current studies of HOTQI are mainly based on electronic systems. Photonic systems are only recently studied based on the 2D Thue-Morse structure [42], but the structure is not a quasi-periodic lattice but arranged in a square lattice. The connection between higher-order topology (HOT) and the complete quasi-periodic structure in photonic and phononic systems has yet to be established. In addition, HOTQI has only been experimentally observed in electrical circuits [43], and it is still a challenge to realize HOTQI experimentally in photonic and phononic systems.

In this Letter, the Stampfli-type and Stampfli-ring-type HOTQIs in electronic, photonic and phononic systems are proposed. Only NNCs are considered, the non-0D TCSs arrays with polyline-shaped distribution at the outer boundary and ring-shaped distribution at the inner boundary are found. The universal theoretical framework of the multimer analysis method (MAM) is improved and the difference in the average charge density (ACD) is proposed as the real-space topological index, which characterizes the unconventional HOT. Furthermore, two HOTQIs and their TCSs arrays are experimentally demonstrated in photonic system.

2. Model and theory

Using an iterative subdivision method, with squares and regular triangles as primitive tiles, a Stampfli-type quasicrystal tiling can be constructed (see Sec. I in Ref. [44]). The vertex of each primitive tile (i.e., the lattice site of quasicrystal) is used as a basic cell. Since the Stampfli-type quasicrystal satisfies C_6 symmetry, considering the interaction between adjacent basic cells, each basic cell contains six subsites. Subsites can set scatterers corresponding to electronics, photonics and phononics. By removing seven basic cells in the center region of Stampfli-type quasicrystal, Stampfli-ring-type quasicrystal can be constructed. The unconventional HOTs in Stampfli-type and Stampfli-ring-type quasicrystals are investigated, as shown in Fig. 1.

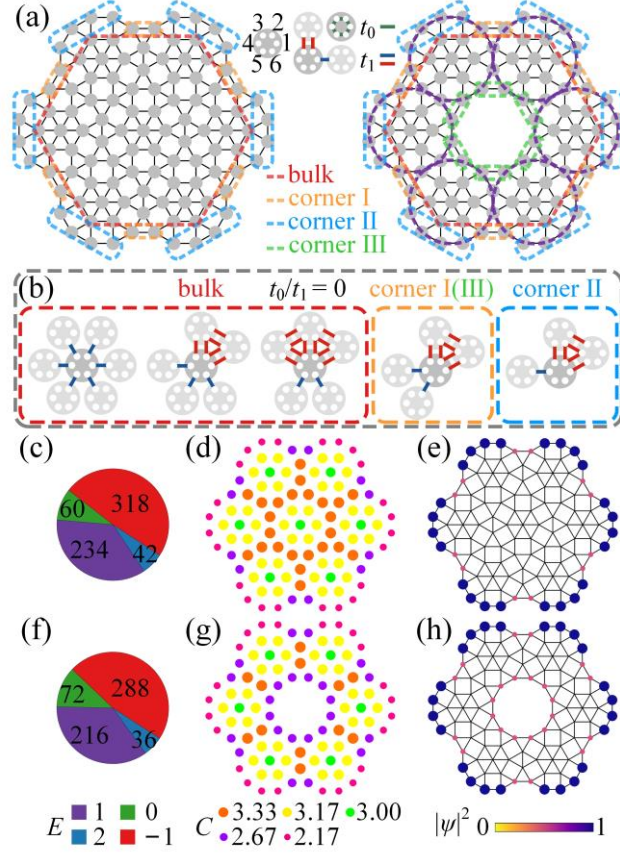


Fig. 1. Stampfli-type and Stampfli-ring-type HOTQIs. (a) The tight-binding models of Stampfli-type and Stampfli-ring-type quasicrystal, which contain 109 and 102 basic cells respectively. The dashed boxes indicate bulk (red) and corner regions (yellow, blue, and green). Due to the properties of quasicrystals, the corner I region corresponds to the edge region of previous HOTIs, and the corner II region is arranged in a polyline. The Stampfli-ring-type quasicrystal consists of six equivalent units (purple dashed circle). The illustrations are the serial number of subsites in the basic cell and the schematic of NNCs within basic cell (t_0) and between adjacent basic cells (t_1). (b) Multimer types in two quasicrystals. The gray circle represents the basic cell in bulk and corner regions, and the light gray circle represents the adjacent basic cell. Energy spectrum of eigenvalues, charge density and normalized probability distribution of the wave function with the parameters of $t_0 = 0$, $t_1 = 1$ for Stampfli-type HOTQI (c)–(e) and Stampfli-ring-type HOTQI (f)–(h).

As a finite-size system, only NNCs are considered, the tight-binding Hamiltonian of two quasicrystals in Fig. 1(a) can be expressed as

$$H_{\text{Stampfli}} = \sum_i c_i^\dagger t_0 h_0 c_i + \sum_{\langle i,j \rangle} c_i^\dagger t_1 h_1 c_j, \quad (1)$$

where c_i^\dagger represents the electron creation operator of basic cell i , c_i (c_j) represents the electron annihilation operator of basic cell i (j). h_0 (h_1) is determined by NNCs within (between) basic cells, and two quasicrystals satisfy the long-range C_{12} symmetry dominated by C_6 symmetry (see Sec. II in Ref. [44]).

When t_0 (t_1) = 0 and t_1 (t_0) \neq 0, the tight-binding model behaves as a combination of multimers (see Sec. III in Ref. [44]). According to the symmetry of two quasicrystals, there are hexamers, trimers, dimers, and monomers. When t_0 = 0 and t_1 = 1, the specific forms of multimers in two quasicrystals are shown in Fig. 1(b). The two quasicrystals have 1 (2) monomer in each basic cell of the corner I (II) region, while there are no monomers in bulk regions. For Stampfli-ring-type quasicrystal, the multimer type in corner I region is consistent with that in corner III region.

The energy spectrum (E) of eigenvalues is obtained by solving H_{Stampfli} . The two quasicrystals have 60 and 72 zero-energy states, respectively, as shown in Figs. 1(c) and 1(f). Filling the band with $E < 0$, the charge density (C) is shown in Figs. 1(d) and 1(g). The corner charge density is different from the bulk charge density, this corner anomaly reflects the HOT [7,8,39,40]. From the probability distribution of wave function in Figs. 1(e) and 1(h), it can be found that there are TCSs protected by the symmetry of two quasicrystals in corner regions, which is a sign that two quasicrystals possess HOT, indicating the realization of two HOTQIs. Interestingly, quite unlike the conventional TCSs, there are TCSs arrays with polyline-shaped distribution at outer boundaries in two quasicrystals, which contain 8 TCSs in the 4 basic cells of each corner II region. Stampfli-ring-type HOTQI also possesses TCSs array with ring-shaped distribution at inner boundary (12 TCSs in corner III regions). The non-0D TCSs arrays break through the limitation of the bulk-edge-corner correspondence (corresponding dimension is 2D-1D-0D), which can exist at outer and inner boundaries, highlighting the unconventional nature of HOTQI.

The corner anomaly was used as a real-space topological index in previous studies of HOTI [7,8]. In this Letter, the relationship between charge density and multimer type is demonstrated by improving the theoretical framework of MAM (see Secs. III–V in Ref. [44]). For the band $E < 0$, the ACD of the subsites corresponding to non-monomers

in the structure is

$$\text{ACD}_0 = \frac{1}{S_0} \sum_{s=1}^{S_0} \sum_{\alpha=1}^N |\psi_s^\alpha|^2, \quad (2)$$

and the ACD of the subsites corresponding to monomers in corner I (II) regions is

$$\text{ACD}_{1(2)} = \frac{1}{S_{1(2)}} \sum_{s=1}^{S_{1(2)}} \sum_{\alpha=1}^N |\psi_s^\alpha|^2, \quad (3)$$

where ψ_s^α is the amplitude at the subsite s for the eigenstate α . N is the total number of eigenstates below the band gap. $S_{1(2)}$ is the total number of subsites corresponding to monomers in corner I (II) regions. The $S_{1(2)}$ of two quasicrystals are 12 (48) and 24 (48), respectively. Since the multimer types in corner I region and corner III region in Stampfli-ring-type HOTQI are consistent, S_1 is the sum of the number of monomers in the two regions. S_0 is the total number of subsites corresponding to non-monomers. The S_0 of two quasicrystals are 594 and 540, respectively.

When the system is in trivial phase, the ACD of any subsite in the system is basically the same and it is completely consistent at $t_1/t_0 \sim 0$. When the system is in topological phase, the electrons below the band gap are mainly filled in the non-monomers, and the ACD of the subsite corresponding to monomer is basically 0. When $t_0/t_1 \sim 0$, it is completely 0. This is because only zero-energy ($E = 0$) electrons can be filled in monomers (see Secs. III and IV in Ref. [44]). $E = 0$ is in the band gap, so the non-zero-energy electrons below the band gap cannot be filled in the monomer, making its ACD = 0. The difference between ACD_0 and $\text{ACD}_{1(2)}$ can be used as a real-space topological index to effectively characterize the topology of the system, which can be expressed as

$$\Delta\text{ACD} = \frac{\text{ACD}_0 - \text{ACD}_{1(2)}}{\max(\text{ACD}_0) - \min(\text{ACD}_{1(2)})}, \quad (4)$$

where ΔACD is normalized, $\max(\text{ACD}_0) = N$, $\min(\text{ACD}_{1(2)}) = 0$. The ΔACD is 0 (non-0) corresponding to the trivial (topological) phase, and the gapless metallic region with ΔACD close to 0 is not contained. The variation of ΔACD with t_0 and t_1 is shown in Fig. 2.

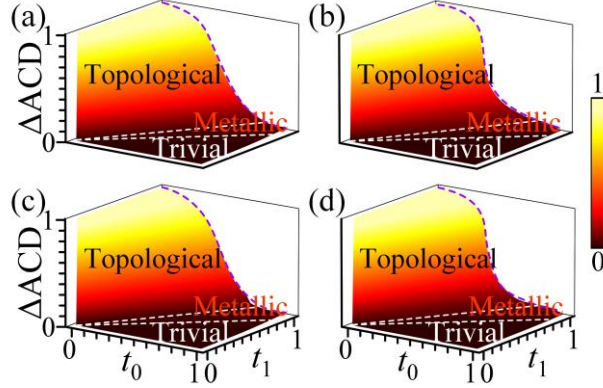


Fig. 2. The variation of ΔACD with t_0 and t_1 . ΔACD for ACD_0 and ACD_1 : (a) Stampfli-type quasicrystal. (c) Stampfli-ring-type quasicrystal. ΔACD for ACD_0 and ACD_2 : (b) Stampfli-type quasicrystal. (d) Stampfli-ring-type quasicrystal.

For Stampfli-type quasicrystals, comparing Figs. 2(a) and 2(b), considering $t_1=1$ and t_0 is decreasing (i.e., t_1/t_0 increases), the variation of the two ΔACDs (purple dashed line) is not consistent. In Fig. 2(a), the growth trend of ΔACD is relatively flat, while in Fig. 2(b), ΔACD increases significantly when t_1/t_0 is large, which indicates that with the increase of t_1/t_0 , the TCSs of corner I region will appear earlier than that of corner II region, which is consistent with the order of TCS appearing after topological edge state in previous HOTI. The ΔACD in Stampfli-ring-type quasicrystal is consistent with Stampfli-type quasicrystal, as shown in Figs. 2(c) and 2(d). MAM and ΔACD provide an effective way to characterize the HOT of various systems. The HOTIs and HOTQIs with different symmetries are further investigated (see Secs. V and VI in Ref. [44]).

3. Results and discussion

Based on the theoretical model of electronic system, two photonic analogues of HOTQIs (i.e., photonic HOTQIs) are further simulated and experimentally demonstrated. The Stampfli-type photonic HOTQI is shown in Fig. 3.

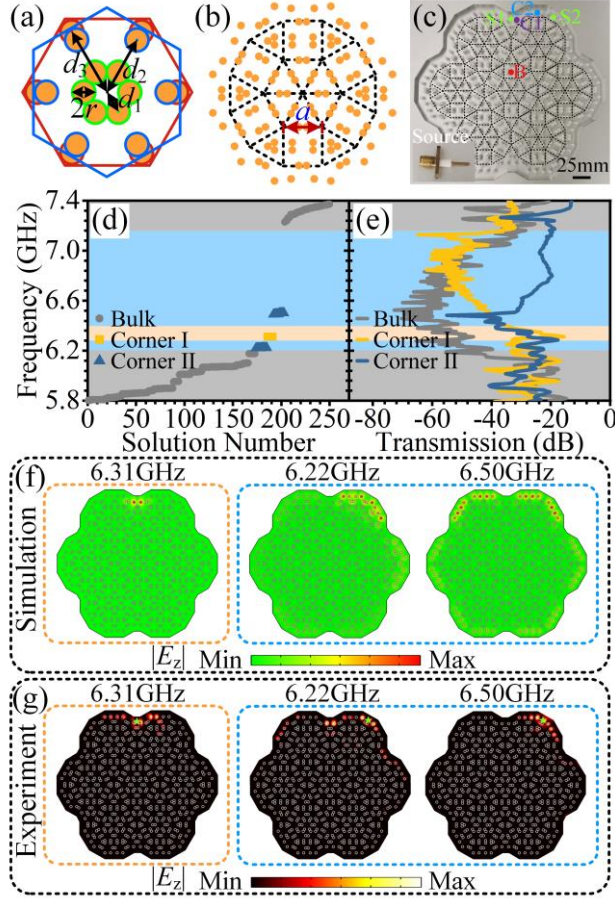


Fig. 3. Stampfli-type photonic HOTQI. (a)–(c) Schematic of the basic cell, schematic of 19 basic cells and photograph of the sample. The scatterer material is zirconia ceramic ($\epsilon_{rl} = 26$), the radius is $r = 2.5$ mm, the height is 10 mm. The distance between adjacent basic cells is $a = 25$ mm, and the distance d ($d = d_1, d_2, d_3$) between the scatterer and the center of basic cell corresponds to different multimers, $d_1 = 2r$ (hexamer), $d_2 = a/2-r$ (dimer), and $d_3 = (a-2r)/\sqrt{3}$ (trimer). The black dashed frame shows the quasicrystal structure. (d) The simulated eigenfrequency distribution. (e) The measured transmission spectrum. The excitation sources are located at S1 and S2, and the probes are located at B, C1 and C2 in Fig. 3(c). The TCSs in corner I and corner II regions from eigenstate simulation (f) and experimental measurement (g). The green pentagram marks the position of excitation source.

As shown in Figs. 3(a)–3(c), based on the tight-binding model of Stampfli-type quasicrystal in Fig. 1(a), six dielectric scatterers are placed at six subsites in each basic cell. The distance between the scatterer and the center of the basic cell is adjusted to construct the multimers (see Sec. VII in Ref. [44]). Different from the previous HOTIs

using crystal as the trivial cladding in simulation and experiment, this Letter uses metal (perfect electric conductors) as the trivial cladding to make the structure more compact (experimental set-ups are detailed in Sec. VIII [44]). From Figs. 3(d) and 3(e), there are TCSs corresponding to monomers of two corner regions in the band gap range of $f \in [6.20 \text{ GHz}, 7.16 \text{ GHz}]$ (see Sec. IX in Ref. [44]). The electric field distribution is further observed, as shown in Figs. 3(f) and 3(g). The simulation and experimental results are in good agreement, and the TCSs array (including 8 TCSs) with polyline-shaped distribution in corner II region of the outer boundary demonstrates the theoretical model.

The Stampfli-ring-type photonic HOTQI is further investigated, as shown in Fig. 4.

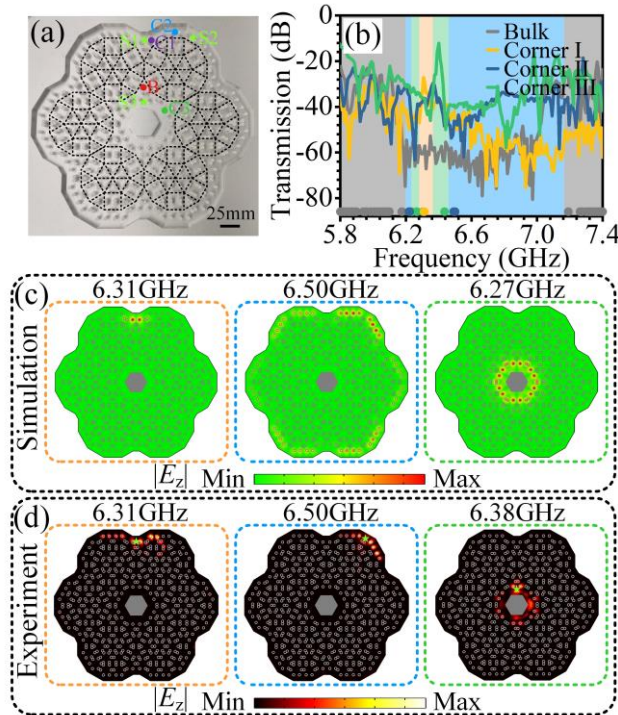


Fig. 4. Stampfli-ring-type photonic HOTQI. (a) Photograph of the sample. 7 basic units in the central region are removed and a hexagonal metal prism is placed. The black dashed frame shows the quasicrystal structure. (b) The measured transmission spectrum. The excitation sources are located at S1, S2 and S3, and the probes are located at B, C1, C2 and C3 in Fig. 4(a). The gray, yellow, blue, and green dots on the horizontal axis correspond to simulated eigenfrequencies of bulk and corner states. The TCSs in corner I, corner II, and corner III regions from eigenstate simulation (c) and experimental measurement (d). The green pentagram marks the position of excitation source.

From Fig. 4(b), there are TCSs corresponding to monomers of three corner regions in the band gap range of $f \in [6.20 \text{ GHz}, 7.16 \text{ GHz}]$. The electric field distribution is shown in Figs. 4(c) and 4(d). In the corner II region of the outer boundary, there is a TCSs array (including 8 TCSs) with polyline-shaped distribution, and in the corner III region of the inner boundary, there is a TCSs array (including 12 TCSs) with ring-shaped distribution, which demonstrates the theoretical model. Compared with the Stampfli-type photonic HOTQI, although 7 basic cells are removed from the bulk region, the TCSs in corner I and corner II regions remain unchanged, reflecting the topological robustness of photonic HOTQI (see Sec. X in Ref. [44]).

In addition to photonic HOTQIs, the phononic HOTQI based on MAM is demonstrated and TCSs arrays at the outer boundary are realized (see Sec. XI in Ref. [44]). Photonic and phononic HOTQIs have extraordinary application potential such as high-efficiency lossless waveguides [45–47], lasers [48–50], and audio lasing [51] due to their highly integrated and multi-region distributed TCSs arrays.

4. Conclusion

In this Letter, the non-0D TCSs arrays with polyline-shaped and ring-shaped distribution at the outer and inner boundaries in Stampfli-type and Stampfli-ring-type HOTQIs are demonstrated through consistent theory, simulations, and experiments. The universal theoretical framework of MAM has been improved and the real-space topological index has been proposed. The unconventional HOTs of two quasicrystals in electronic, photonic and phononic systems have been characterized qualitatively and quantitatively. The photonic and phononic HOTQIs realized in this work broaden the classification of HOTI, which provide a fresh perspective for designing photonic and phononic devices with stronger localization and higher integration degree.

Acknowledgements

The authors thank Xiaokang Dai for helpful discussions. The authors acknowledge Professor J. Q. Liu for software sponsorship. J. Liu acknowledges the National Natural Science Foundation of China (Grants No. 61405058 and 62075059), the Natural Science Foundation of Hunan Province (Grants No. 2017JJ2048 and 2020JJ4161), the

Scientific Research Foundation of Hunan Provincial Education Department (Grant No. 21A0013), and the Fundamental Research Funds for the Central Universities (Grant No. 531118040112). F. Gao and X. Lin acknowledge the support partly from the National Natural Science Fund for Excellent Young Scientists Fund Program (Overseas) of China, the Key Research and Development Program of the Ministry of Science and Technology (Grants No. 2022YFA1404704, 2022YFA1405200, and 2022YFA1404902), the National Natural Science Foundation of China (Grants No. 61975176 and 62175212), the Key Research and Development Program of Zhejiang Province (Grant No. 2022C01036), Zhejiang Provincial Natural Science Fund Key Project (Grant No. Z23F050009), and the Fundamental Research Funds for the Central Universities (Grant No. 2021FZZX001-19).

References

- [1] W. A. Benalcazar, B. A. Bernevig, and T. L. Hughes, “Quantized electric multipole insulators,” *Science* **357**(6346): 61–66 (2017).
- [2] W. A. Benalcazar, B. A. Bernevig, and T. L. Hughes, “Electric multipole moments, topological multipole moment pumping, and chiral hinge states in crystalline insulators,” *Phys. Rev. B* **96**(24): 245115 (2017).
- [3] J. Langbehn, Y. Peng, L. Trifunovic, F. von Oppen, and P. W. Brouwer, “Reflection-symmetric second-order topological insulators and superconductors,” *Phys. Rev. Lett.* **119**(24): 246401 (2017).
- [4] Z. Song, Z. Fang, and C. Fang, “(d–2)-dimensional edge states of rotation symmetry protected topological states,” *Phys. Rev. Lett.* **119**(24): 246402 (2017).
- [5] F. Schindler, A. M. Cook, M. G. Vergniory, Z. Wang, S. S. P. Parkin, B. A. Bernevig, and T. Neupert, “Higher-order topological insulators,” *Sci. Adv.* **4**(6): eaat0346 (2018).
- [6] M. Ezawa, “Higher-order topological insulators and semimetals on the breathing kagome and pyrochlore lattices,” *Phys. Rev. Lett.* **120**(2): 026801 (2018).
- [7] W. A. Benalcazar, T. Li, and T. L. Hughes, “Quantization of fractional corner charge in C_n -symmetric higher-order topological crystalline insulators,” *Phys. Rev.*

- B **99**(24): 245151 (2019).
- [8] C. W. Peterson, T. Li, W. A. Benalcazar, T. L. Hughes, and G. Bahl, “A fractional corner anomaly reveals higher-order topology,” *Science* **368**(6495): 1114–1118 (2020).
 - [9] B. Xie, H.-X. Wang, X. Zhang, P. Zhan, J.-H. Jiang, M. Lu, and Y. Chen, “Higher-order band topology,” *Nat. Rev. Phys.* **3**(7): 520–532 (2021).
 - [10] B.-Y. Xie, H.-F. Wang, H.-X. Wang, X.-Y. Zhu, J.-H. Jiang, M.-H. Lu, and Y.-F. Chen, “Second-order photonic topological insulator with corner states,” *Phys. Rev. B* **98**(20): 205147 (2018).
 - [11] X.-D. Chen, W.-M. Deng, F.-L. Shi, F.-L. Zhao, M. Chen, and J.-W. Dong, “Direct observation of corner states in second-order topological photonic crystal slabs,” *Phys. Rev. Lett.* **122**(23): 233902 (2019).
 - [12] B.-Y. Xie, G.-X. Su, H.-F. Wang, H. Su, X.-P. Shen, P. Zhan, M.-H. Lu, Z.-L. Wang, and Y.-F. Chen, “Visualization of higher-order topological insulating phases in two-dimensional dielectric photonic crystals,” *Phys. Rev. Lett.* **122**(23): 233903 (2019).
 - [13] M. Li, D. Zhirihin, M. Gorlach, X. Ni, D. Filonov, A. Slobozhanyuk, A. Alù, and A. B. Khanikaev, “Higher-order topological states in photonic kagome crystals with long-range interactions,” *Nat. Photon.* **14**(2): 89–94 (2020).
 - [14] J. Jiang, B. Yan, Y. Peng, J. Xie, A. Shi, and J. Liu, “Multiband topological states in non-Hermitian photonic crystals,” *Opt. Lett.* **47**(2): 437–440 (2022).
 - [15] Y. Peng, E. Liu, B. Yan, J. Xie, A. Shi, P. Peng, H. Li, and J. Liu, “Higher-order topological states in two-dimensional Stampfli-Triangle photonic crystals,” *Opt. Lett.* **47**(12): 3011–3014 (2022).
 - [16] Q. Xu, Y. Peng, B. Yan, A. Shi, P. Peng, J. Xie, and J. Liu, “Multiband topological states in the Penrose-triangle photonic crystals,” *Opt. Lett.* **48**(1): 101–104 (2023).
 - [17] H. Xue, Y. Yang, F. Gao, Y. Chong, and B. Zhang, “Acoustic higher-order topological insulator on a kagome lattice,” *Nat. Mater.* **18**(2): 108–112 (2019).
 - [18] Z. Zhang, M. R. López, Y. Cheng, X. Liu, and J. Christensen, “Non-Hermitian sonic second-order topological insulator,” *Phys. Rev. Lett.* **122**(19): 195501 (2019).
 - [19] S. Zheng, X. Man, Z.-L. Kong, Z.-K. Lin, G. Duan, N. Chen, D. Yu, J.-H. Jiang,

- and B. Xia, “Observation of fractal higher-order topological states in acoustic metamaterials,” *Sci. Bull.* **67**(20): 2069–2075 (2022).
- [20] J. Li, Q. Mo, J.-H. Jiang, and Z. Yang, “Higher-order topological phase in an acoustic fractal lattice,” *Sci. Bull.* **67**(20): 2040–2044 (2022).
- [21] X.-C. Sun, H. Chen, H.-S. Lai, C.-H. Xia, C. He, Y.-F. Chen, “Ideal acoustic quantum spin Hall phase in a multi-topology platform,” *Nat. Commun.* **14**(1): 952 (2023).
- [22] A. Cerjan, M. Jürgensen, W. A. Benalcazar, S. Mukherjee, and M. C. Rechtsman, “Observation of a higher-order topological bound state in the continuum,” *Phys. Rev. Lett.* **125**(21): 213901 (2020).
- [23] L. Liu, T. Li, Q. Zhang, M. Xiao, and C. Qiu, “Universal mirror-stacking approach for constructing topological bound states in the continuum,” *Phys. Rev. Lett.* **130**(10): 106301 (2023).
- [24] L. Ye, C. Qiu, M. Xiao, T. Li, J. Du, M. Ke, and Z. Liu, “Topological dislocation modes in three-dimensional acoustic topological insulators,” *Nat. Commun.* **13**(1): 508 (2022).
- [25] C. W. Peterson, T. Li, W. Jiang, T. L. Hughes, and G. Bahl, “Trapped fractional charges at bulk defects in topological insulators,” *Nature* **589**(7842): 376–380 (2021).
- [26] Y. Liu, S. Liang, F.-F. Li, Z.-K. Lin, X. Tao, Y. Poo, and J.-H. Jiang, “Bulk-disclination correspondence in topological crystalline insulators,” *Nature* **589**(7842): 381–385 (2021).
- [27] Y. Deng, W. A. Benalcazar, Z.-G. Chen, M. Oudich, G. Ma, and Y. Jing, “Observation of degenerate zero-energy topological states at disclinations in an acoustic lattice,” *Phys. Rev. Lett.* **128**(17): 174301 (2022).
- [28] Z.-K. Lin, Y. Wu, B. Jiang, Y. Liu, S.-Q. Wu, F. Li, and J.-H. Jiang, “Topological Wannier cycles induced by sub-unit-cell artificial gauge flux in a sonic crystal,” *Nat. Mater.* **21**(4): 430–437 (2022).
- [29] W. A. Benalcazar and A. Cerjan, “Chiral-symmetric higher-order topological phases of matter,” *Phys. Rev. Lett.* **128**(12): 127601 (2022).

- [30] M. A. Bandres, M. C. Rechtsman, and M. Segev, “Topological photonic quasicrystals: fractal topological spectrum and protected transport,” *Phys. Rev. X* **6**(1): 011016 (2016).
- [31] H. Huang and F. Liu, “Quantum spin Hall effect and spin Bott index in a quasicrystal lattice,” *Phys. Rev. Lett.* **121**(12): 126401 (2018).
- [32] Z. Che, Y. Zhang, W. Liu, M. Zhao, J. Wang, W. Zhang, F. Guan, X. Liu, W. Liu, L. Shi, and J. Zi, “Polarization singularities of photonic quasicrystals in momentum space,” *Phys. Rev. Lett.* **127**(4): 043901 (2021).
- [33] J. Fan and H. Huang, “Topological states in quasicrystals,” *Front. Phys.* **17**(1): 13203 (2022).
- [34] Y. Zhang, Z. Lan, L. Hu, Y. Shu, X. Yuan, P. Guo, X. Peng, W. Chen, and J. Li, “Chiral photonic topological states in Penrose quasicrystals,” *Opt. Lett.* **48**(9): 2229–2232 (2023).
- [35] D. Varjas, A. Lau, K. Pöyhönen, A. R. Akhmerov, D. I. Pikulin, and I. C. Fulga, “Topological phases without crystalline counterparts,” *Phys. Rev. Lett.* **123**(19): 196401 (2019).
- [36] R. Chen, C.-Z. Chen, J.-H. Gao, B. Zhou, and D.-H. Xu, “Higher-order topological insulators in quasicrystals,” *Phys. Rev. Lett.* **124**(3): 036803 (2020).
- [37] C.-B. Hua, R. Chen, B. Zhou, and D.-H. Xu, “Higher-order topological insulator in a dodecagonal quasicrystal,” *Phys. Rev. B* **102**(24): 241102(R) (2020).
- [38] S. Spurrier and N. R. Cooper, “Kane-Mele with a twist: Quasicrystalline higher-order topological insulators with fractional mass kinks,” *Phys. Rev. Research* **2**(3): 033071 (2020).
- [39] H. Huang, J. Fan, D. Li, and F. Liu, “Generic orbital design of higher-order topological quasicrystalline insulators with odd five-fold rotation symmetry,” *Nano Lett.* **21**(16): 7056–7062 (2021).
- [40] C. Wang, F. Liu, and H. Huang, “Effective model for fractional topological corner modes in quasicrystals,” *Phys. Rev. Lett.* **129**(5): 056403 (2022).
- [41] S. Traverso, M. Sassetti, and N. T. Ziani, “Role of the edges in a quasicrystalline Haldane model,” *Phys. Rev. B* **106**(12): 125428 (2022).

- [42] L. Xiong, Y. Zhang, Y. Liu, Y. Zheng, and X. Jiang, “Higher-order topological states in photonic Thue-Morse quasicrystals: quadrupole insulator and the origin of corner states,” *Phys. Rev. Applied* **18**(6): 064089 (2022).
- [43] B. Lv, R. Chen, R. Li, C. Guan, B. Zhou, G. Dong, C. Zhao, Y. Li, Y. Wang, H. Tao, J. Shi, and D.-H. Xu, “Realization of quasicrystalline quadrupole topological insulators in electrical circuits,” *Commun. Phys.* **4**(1): 108 (2021).
- [44] See Supplementary Material for details of construction of Stampfli-type quasicrystal tiling, Hamiltonian and symmetry of Stampfli-type quasicrystal, the universal theoretical framework of MAM, the role of monomer in Hamiltonian, MAM to analyze NIs and HOTIs satisfying C_4 and C_6 symmetry, HOTQIs with different symmetries, construction of the photonic HOTQI, experimental set-ups and methods, bandgap of photonic NI, robustness of photonic HOTQI, and MAM to analyze phononic quasicrystals.
- [45] J. Lu, C. Qiu, L. Ye, X. Fan, M. Ke, F. Zhang, and Z. Liu, “Observation of topological valley transport of sound in sonic crystals,” *Nat. Phys.* **13**(4): 369–374 (2017).
- [46] B. Yan, Y. Peng, J. Xie, Y. Peng, A. Shi, H. Li, F. Gao, P. Peng, J. Jiang, F. Gao, J. Liu, and S. Wen, “Multifrequency and multimode topological waveguides in Stampfli-triangle photonic crystal with large valley Chern numbers,” arXiv: 2104.14142.
- [47] Y.-L. Hong, G.-H. Tang, R.-W. Peng, R.-H. Fan, Z.-L. Ma, Z. Wang, Y. Jiang, L.-D. Chen, and M. Wang, “Direct observation of terahertz topological valley transport,” *Opt. Express* **30**(9): 14839–14850 (2022).
- [48] Y. Zeng, U. Chattopadhyay, B. Zhu, B. Qiang, J. Li, Y. Jin, L. Li, A. G. Davies, E. H. Linfield, B. Zhang, Y. Chong, and Q. J. Wang, “Electrically pumped topological laser with valley edge modes,” *Nature* **578**(7794): 246–250 (2020).
- [49] Z.-K. Shao, H.-Z. Chen, S. Wang, X.-R. Mao, Z.-Q. Yang, S.-L. Wang, X.-X. Wang, X. Hu, and R.-M. Ma, “A high-performance topological bulk laser based on band-inversion-induced reflection,” *Nat. Nanotechnol.* **15**(1): 67–72 (2020).
- [50] L. Yang, G. Li, X. Gao, and L. Lu, “Topological-cavity surface-emitting laser,” *Nat.*

- Photon. **16**(4): 279–283 (2022).
- [51] B. Hu, Z. Zhang, H. Zhang, L. Zheng, W. Xiong, Z. Yue, X. Wang, J. Xu, Y. Cheng, X. Liu, and J. Christensen, “Non-Hermitian topological whispering gallery,” Nature, **597**(7878): 655–659 (2021).